

Templated Non-Oxide Sol-Gel Preparation of Well-Ordered Macroporous (inverse opal) Ta_3N_5 Films

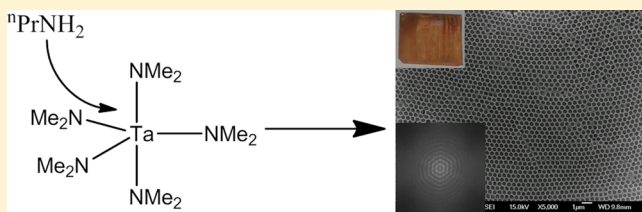
Christopher F. Mallinson,[†] Benjamin M. Gray,[†] Andrew L. Hector,*^{*,†} Martyn A. McLachlan,[‡] and John R. Owen[†]

[†]Chemistry, University of Southampton, Southampton SO17 1BJ, United Kingdom

[‡]Department of Materials and Centre for Plastic Electronics, Imperial College London, Exhibition Road, London, SW7 2AZ, United Kingdom

Supporting Information

ABSTRACT: Reactions of $Ta(NMe_2)_5$ and *n*-propylamine are shown to be an effective system for sol-gel processing of Ta_3N_5 . Ordered macroporous films of Ta_3N_5 on silica substrates have been prepared by infiltration of such a sol into close-packed sacrificial templates of cross-linked 500 nm polystyrene spheres followed by pyrolysis under ammonia to remove the template and crystallize the Ta_3N_5 . Templates with long-range order were produced by controlled humidity evaporation. Pyrolysis of a sol-infiltrated template at 600 °C removes the polystyrene but does not crystallize Ta_3N_5 , and X-ray diffraction shows nanocrystalline TaN plus amorphous material. Heating at 700 °C crystallizes Ta_3N_5 while retaining a high degree of pore ordering, whereas at 800 °C porous films with a complete loss of order are obtained.



INTRODUCTION

Inverse opal architectures have been produced in a wide range of materials due to potential applications as photonic band gap materials,¹ battery electrodes,² gas sensors,³ catalysts,^{4–6} membranes,⁷ and biomaterials.⁸ These materials are usually synthesized using close-packed arrays of polymer or silica spheres as sacrificial templates. The void space between the spheres is typically infiltrated with precursors of the target material and the template spheres subsequently removed by thermal processing, solvent extraction, or chemical etching. The most intensively studied inverse opal materials are metals, binary oxides, such as SiO_2 , TiO_2 , Al_2O_3 , and ZrO_2 ,^{9,10} ternary transition/main group metal oxides,¹¹ semiconductors,¹² and carbon.²

There are only a few examples of nitride materials with inverse opal structures. For example, $SiCN$ has been obtained using a polysilazane preceramic precursor templated around silica spheres and was proposed as a catalyst support for high-temperature fuel reforming owing to its surface geometry and good stability up to 1200 °C.⁵ Very high quality inverse opals of WN^{13} and $Ta_3N_5^{14}$ have been produced by atomic layer deposition also using silica sphere templates, though this method is not suited to large-scale applications, and an aggressive HF etching process is required to remove the template. There are a small number of examples of conversion of inverse opal powders to metal nitrides. Graphitic carbon nitride obtained by templating cyanamide around silica spheres has been converted to a TiN/C composite powder with inverse opal structure by high-temperature reaction with $TiCl_4$.¹⁵ These were suggested as catalyst supports, and $Ti_{0.7}W_{0.3}N$ has similarly been produced from the oxide for the same

application.¹⁶ Ta_3N_5 inverse opal powders have been obtained by a templated sol-gel synthesis of the porous oxide powder followed by nitridation, and these materials were studied as photocatalysts for water splitting.⁶

Conversion of oxides to nitrides is often an aggressive high-temperature process, and we previously developed a nonoxide sol-gel route to TiN inverse opals¹⁷ using cross-linked polystyrene spheres and infiltrating using an amide-derived sol precursor, chemistry that previously we also used to directly access TiN films.¹⁸ The relatively gentle conditions used in this method have the potential to produce inverse opal nitride films on a range of substrates, e.g., for use as fuel cell or battery electrodes, optical materials, or photocatalysts. Nonoxide sol-gel routes could also produce a variety of structured and porous metal nitride materials,¹⁹ as demonstrated in the more extensively studied silicon nitride system where films,²⁰ membranes,²¹ aerogels,^{22,23} inverse opals,¹⁷ and molecule-templated microporous catalysts²⁴ have been reported. Hence, expansion of our TiN processing route to other metals is an important target of our research program.

Ta_3N_5 has been the focus of many recent investigations due to its high photocatalytic activity with visible light.²⁵ The most intense region of the solar spectrum is centered at 2.6 eV, and Ta_3N_5 has a band gap of ~2.1 eV,²⁶ hence, it could potentially utilize more than 45% of the incident solar energy.²⁷ Materials investigated range from films²⁸ and powders²⁹ to nanoparticles³⁰ and nanotube arrays.³¹ Recently, a study on nanoporous Ta_3N_5 films showed high activity with high surface

Received: May 21, 2013

Published: August 15, 2013

area porous structures as photoanodes to oxidize water,³² raising the possibility of separated oxygen and hydrogen generation.

Here we report the synthesis of Ta_3N_5 inverse opal films using a nonoxide sol-gel process based on $Ta(NMe_2)_5$ cross-linked by propylamine. This sol is infiltrated into a template formed of hexagonal close-packed 500 nm cross-linked polystyrene spheres before firing in ammonia to crystallize the Ta_3N_5 and calcine the template. The template-forming method has been improved relative to our TiN and SiN_x inverse opal preparations¹⁷ by employing methods previously developed for photonic crystals¹⁰ to produce large ordered domains of inverse opal.

EXPERIMENTAL SECTION

All sol preparations and infiltrations were carried out under dry N_2 using glovebox or Schlenk line conditions. Hexane was distilled from sodium–benzophenone and *n*-propylamine from BaO; both were stored under dry N_2 . $Ta(NMe_2)_5$ was obtained from SAFC Hitech and used as supplied. Gaseous ammonia (Air Products anhydrous grade) was dried by passing through a column of dry 3 Å molecular sieves.

Templates were produced on $12 \times 50 \times 1$ mm silica tiles. These were cleaned by sonication in saturated $KOH_{(aq)}$, H_2O , propan-2-ol, and acetone before drying with a stream of dry N_2 . Divinylbenzene cross-linked, amidine-capped polystyrene spheres (Invitrogen, 41 cm³ of 0.1% suspension in deionized water) were sonicated for 10 min to ensure an even dispersion and used to produce a batch of 7 templates. A cleaned silica tile was placed into a 25 mm diameter specimen tube such that it formed an angle of $\sim 70^\circ$ to the base of the tube. The polystyrene suspension (6 cm³) was then carefully syringed into the base of the tube. Seven of these were equally spaced on an insulating tray with an eighth tube containing water (6 cm³) to moderate the humidity. The tray was then carefully placed into an oven at 65 ± 1 °C. As the water evaporated to dryness a striated, opalescent film of PS beads formed. These templates were then dried, removed from the vials, stored in a desiccator, and then further dried under vacuum before use.

Sols were produced in hexane due to a previous finding that the cross-linked PS spheres were stable in it.¹⁷ $Ta(NMe_2)_5$ (4.013 g, 10 mmol) was dissolved in dry hexane (7.5 cm³), and ¹⁰PrNH₂ (1.64 cm³, 20 mmol) was injected slowly. Gas evolution was observed. Stirring continued at room temperature for ~ 15 h, during which the sol darkened slightly but remained a clear, yellow solution. The sol was infiltrated into the PS arrays by submerging ~ 1 –2 mm of the edge of the tiles into the sol in the glovebox so that the liquid was drawn in by capillary action and the solvent could then evaporate from the surface. The tiles were left to infiltrate for 1 h, over which time period the volume reduced to around 20% of its original value, and then removed and allowed to dry for 2 h.

The infiltrated arrays were heated under a flow of dry ammonia to 600, 700, or 800 °C at 1 °C min⁻¹ and held for 10 h before cooling to room temperature at 5 °C min⁻¹. For comparison, continuous solid Ta_3N_5 films (i.e., with no template) were produced by dip coating the same silica tiles into the sol and firing under the same conditions as the arrays. Similarly, yellow xerogel samples were also obtained by solvent removal from the infiltration sols in vacuo and then heating under the same conditions to provide bulk samples.

X-ray diffraction (XRD) data were collected using a Bruker C2 Discover with GADDS diffractometer using Cu K α_1 radiation. Scanning electron microscopy (SEM) used a Jeol JSM6500F FEG-SEM or a Philips XL30-ESEM with an EDAX energy-dispersive X-ray (EDX) detector. ¹H NMR spectra were collected with a Bruker AV-300 spectrometer; samples were produced by adding an appropriate molar quantity of *n*-propylamine to a 0.0012 mol dm⁻³ solution of $Ta(NMe_2)_5$ in C_6D_6 , and chemical shifts were corrected by referencing to the benzene ¹H peak ($\delta = 7.26$ ppm). Thermogravimetric analyses (TGA) were obtained with a Mettler Toledo TGA851e with samples in an alumina crucible heated to 800 °C at a rate of 10 °C min⁻¹ under

flowing high-purity nitrogen (80 cm³ min⁻¹ Air Products BiP grade). Combustion microanalyses (C, H, N) were outsourced to Medac and collected using aluminum capsules and a WO_3 combustion aid, conditions that we found previously to provide good combustion of metal nitride samples.

RESULTS AND DISCUSSION

We previously reported the use of a nonoxide sol-gel route to produce TiN inverse opal films using the same divinylbenzene cross-linked, amidine-capped 500 nm polystyrene spheres as the template as are used in this work.¹⁷ Previously the regions of ordered macroporous film were limited to a few micrometers, and one of our key interests in expanding this work to another system was to increase the size of the ordered regions. Large area ordered close-packed arrays of polymer spheres can be produced by self-assembly on a surface at the meniscus of an evaporating suspension of the spheres, and this process can be controlled by changing the concentration of the suspension, the temperature and the humidity of the environment in which the evaporation is being carried out.¹⁰ At 65 °C with a 0.1% suspension of the cross-linked spheres it was possible to obtain arrays of $\sim 1 \times 1.5$ cm as shown in Figure 1. These exhibited

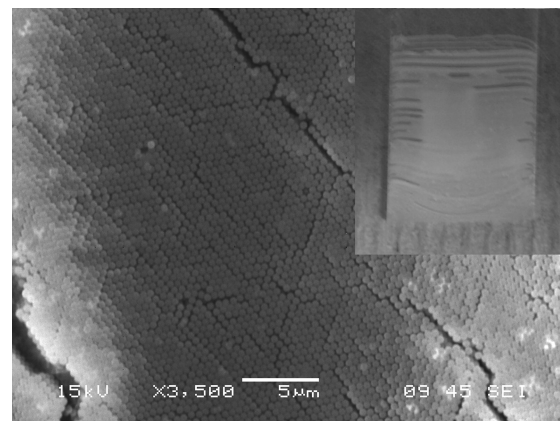
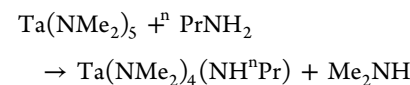


Figure 1. SEM image of a polystyrene sphere template showing overall ordering of the domain orientation, the network of small cracks, and the larger gap between domains (bottom left); (inset) photograph of the whole template on a silica tile with a coated region of $\sim 1 \times 1.5$ cm showing the bulk striations.

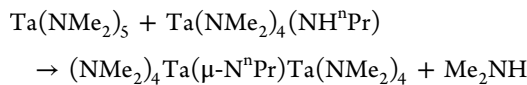
long-range alignment of the orientation of the hexagonal close-packed sphere array, resulting in green opalescence across the entire sample when the template was held at an appropriate viewing angle. They contain cracks along (110) planes in the array due to shrinkage during drying and larger horizontal striations between the macroscopic domains, the size of which (~ 0.5 mm) is competitive with other templates produced in this way.¹⁰

Primary amines can act as the cross-linking agent in nonoxide sol-gel processing to form metal nitrides from metal dialkylamides by transamination of the metal center followed by condensation reactions resulting in bridging alkylamide groups and formation of polymeric species in solution.

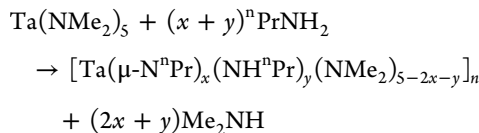
Transamination



Condensation



Overall



Previously we demonstrated this chemistry to be effective for processing of TiN as the sols could be used to deposit films by dip coating or inverse opals by template infiltration, and then the resultant xerogels could be decomposed to TiN by heating in ammonia.^{17,18} The work reported herein is the first example with another metal. With the larger Ta centers there is a higher likelihood that the polymers will also contain some coordinated neutral amine and hence increase the Ta coordination number above the 5-coordinate level assumed in the equations above, but this need not change the behavior for sol-gel processing.

Reactions of $\text{Ta}(\text{NMe}_2)_5$ with ammonia result in precipitation of a polymer with bridging amide groups that decomposes to Ta_3N_5 or TaN on heating in ammonia or inert gases, respectively.^{33,34} These facile reactions are unsuitable for sol-gel processing as precipitation occurs due to formation of large aggregates. Transamination reactions of $\text{Ti}(\text{NMe}_2)_4$ with 2 equiv of primary *n*-alkyl amines also appeared to be facile as the propylamine was not observed in the ^1H NMR spectra after a short period of aging, but the condensation process was well controlled, with a strong color change observed over the first few minutes of reaction but then no precipitation even after the sols had been kept for several days.¹⁸ Condensation was promoted by solvent evaporation as the resulting xerogels were then found to be insoluble. Slow addition of 2 mol equiv of propylamine to a THF or hexane solution of $\text{Ta}(\text{NMe}_2)_5$ resulted in some gas evolution from the solution, presumably loss of the volatile dimethylamine byproduct, but only minor color changes were observed. Larger quantities of propylamine up to 5 mol equiv also did not produce any color changes, and in contrast to the titanium reactions, these larger quantities also did not lead to formation of any precipitate.

In order to better understand the speciation in the tantalum amide-derived sols ^1H NMR spectra were collected on solutions of $\text{Ta}(\text{NMe}_2)_5$ with various quantities of added propylamine; a selection of these are in Figure 2. Propylamine is only observed very weakly in these spectra until sufficient quantities are added to fully displace the dimethylamide groups, as previously observed in the analogous reactions with $\text{Ti}(\text{NMe}_2)_4$. The dimethylamine signal, a doublet at 2.2 ppm, is strong once only 0.7 mol equiv of propylamine has been added to the sol and then remains fairly constant due to vaporization of the excess of this volatile compound and formation of a saturated solution. The $\text{Ta}(\text{NMe}_2)_5$ signal is split by addition of small amounts of amine, presumably due to $\text{Ta}(\text{NMe}_2)_x(\text{NHPr})_y$ species, and becomes very weak beyond ~2 equiv of amine. Broad features at slightly higher δ than those of propylamine could be due to coordinated terminal or bridging propylamide groups. Coordinated groups were not observed with $\text{Ti}(\text{NMe}_2)_4$, and in combination with the lack of precipitate with excess amine and the less obvious changes to

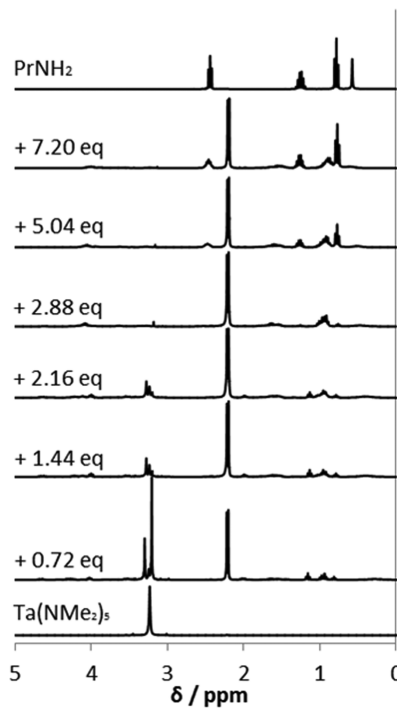


Figure 2. ^1H NMR spectra of $\text{Ta}(\text{NMe}_2)_5$ (bottom), $^n\text{PrNH}_2$ (top), and the products of reactions between $\text{Ta}(\text{NMe}_2)_5$ and the number of molar equivalents of propylamine shown in the labels.

the sol on amine addition, this suggests that condensation occurs less readily in $\text{Ta}(\text{NMe}_2)_5$ -derived sols and that smaller species will be present in solution.

In vacuo removal of solvent from a sol produced from $\text{Ta}(\text{NMe}_2)_5$ and 2 mol equiv of propylamine in THF resulted in a foamy yellow xerogel containing gas bubbles produced by solvent evaporation. Combustion microanalysis of this material gave 22.48% C, 4.82% H, and 9.25% N. The high carbon content is consistent with the expected presence of large numbers of propylamide groups in the gel. After solvent evaporation the gels were found to be insoluble, showing that although condensation was found to be slower in solution than in $\text{Ti}(\text{NMe}_2)_4$ -derived sols it still occurs sufficiently on solvent evaporation to produce a covalently bound network. TGA of the xerogel in nitrogen showed a gradual mass loss of 31% between 100 and 375 °C and then no further mass loss up to 800 °C (Supporting Information). Ammonia cross-linked polymers produced from metal dialkylamides have been shown by mass spectrometry to lose mass in this temperature range associated with continuing condensation reactions accompanied with ammonia and amine loss and then to lose nitrogen with reduction of the metal at higher temperatures.³³ By analogy, it is likely that no reduction of Ta occurs up to 800 °C.

Heating the xerogel in flowing ammonia at 600, 700, or 800 °C resulted in collapse of the foam structure and formation of reddish-black residues; the diffraction patterns obtained from these samples are shown in Figure 3. The material heated to 600 °C was found to be amorphous, while at either 700 or 800 °C the observed diffraction peaks correspond to the normal structure of Ta_3N_5 .^{35,36} Use of the Scherrer formula indicates the observed peak widths correspond to a crystallite size of ~20 nm. The material heated at 800 °C contained 2.34% C, 1.1% H, and 12.86% N (11.4% N calculated for Ta_3N_5), suggesting

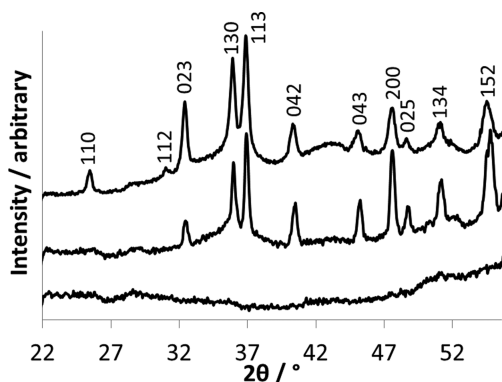


Figure 3. XRD patterns of a bulk $\text{Ta}(\text{NMe}_2)_5$ /propylamine-derived xerogel heated to 600 (bottom), 700 (middle), and 800 °C (top) with the major reflections of the usual orthorhombic Ta_3N_5 structure labeled with Miller indices.^{35,36}

incomplete reaction and possibly some carbon incorporation (also consistent with the color as Ta_3N_5 is bright orange-red). It is possible that the foam structure contains small or poorly interconnected pores and hence restricts access of the ammonia flow to the bulk of the xerogel.

Sols in THF and hexane were also used to produce thin films by dip coating a silica slide to a depth of 20 mm four times in the glovebox and allowing it to dry in between each dipping. The xerogel film coated the substrate smoothly, but on heating the films were observed to crack and become flaky, especially with hexane-based sols. No good quality films after firing were obtained from these sols. In forming TiN films it was found that a longer chain amine, *n*-octylamine, produced better adhered and less cracked films,¹⁸ and this change could be pursued if Ta_3N_5 films were desired. XRD patterns of films fired at 600 °C contained broad peaks at 38° and 44° consistent with cubic TaN . Interestingly, CVD at this temperature from $\text{Ta}(\text{NMe}_2)_5$ and ammonia also yields TaN .³⁷ Increasing the temperature to 700 or 800 °C yielded red films and XRD patterns consistent with Ta_3N_5 . Formation of nanocrystalline TaN at 600 °C and the red color of the films produced at higher temperatures are significant changes in behavior relative to the bulk xerogels, and both could be due to better access to the gel by ammonia in the planar morphology and hence more effective removal of organic ligands during the firing process.

Infiltration of the polystyrene opal templates was achieved by capillary action and evaporation over a 1 h period when the edge of the film was placed into a hexane-based $\text{Ta}(\text{NMe}_2)_5$ /propylamine sol in the glovebox. THF-based sols are unsuitable for this purpose as the template dissolves in THF. The striations shown in Figure 1 prevented effective infiltration from the bottom of the slide, but after infiltration from the side of the slide the yellow color of the xerogel was clearly visible throughout the polystyrene template. The same procedure has been used to produce TiO_2 inverse opals with long-range order.¹⁰ The infiltration time was important to achieving a good quality inverse opal as leaving the material in the sol for too long results in a solid layer of material coating the porous structure; similarly, use of dip coating to fill these templates resulted in a porous structure with a solid coating over the surface. The SEM images in Figure 4 show three of these films after heating in ammonia. Note that the template has been removed cleanly by the heating process and that at 600, 700, and 800 °C the films have retained the pore structure originally introduced by the template. This has a high degree of order at

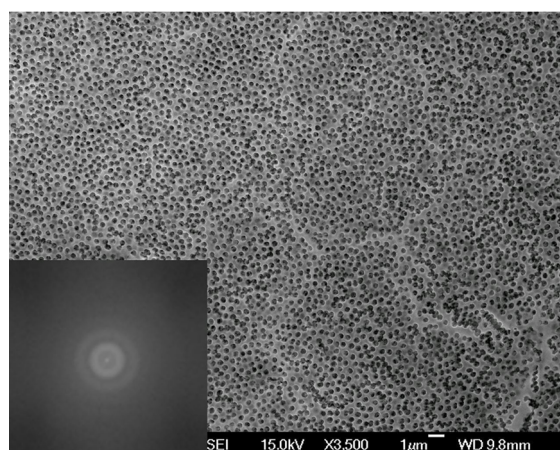
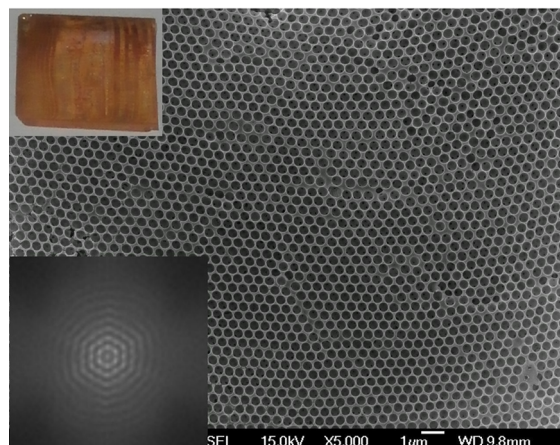
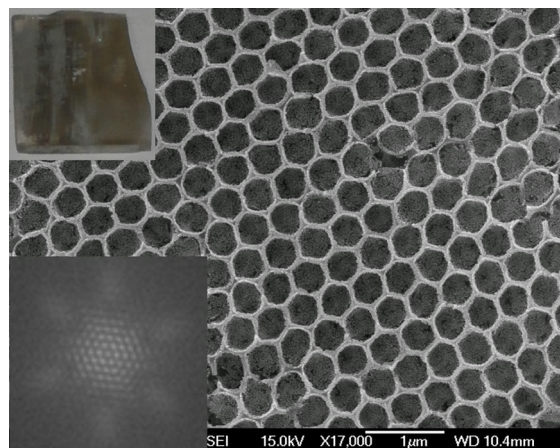


Figure 4. SEM images, photographs (inset), and calculated FFTs (inset) of macroporous films produced by infiltrating a $\text{Ta}(\text{NMe}_2)_5$ /propylamine sol in hexane into a close-packed polystyrene sphere template and heating in ammonia at 600 (top), 700 (middle), and 800 °C (bottom).

600 °C and only a small loss of order at 700 °C, but heating at 800 °C resulted in loss of order in the pore structure as seen in the image and the fast Fourier transform (FFT) and a thickening of the pore walls. We previously found in Ta_3N_5 samples produced by ammonolysis of Ta_2O_5 that the crystallite size only increased at temperatures of 800 °C and above and attributed this to the start of interparticle sintering;³⁶ the same effect is probably operating here.

The porous films produced by heating to 600 °C were black and metallic but displayed green opalescence across the entire film. The highly ordered structure (Figure 4) results in Bragg-type optical diffraction from the periodic spacing of the macroscopic lattice, the length scale and dielectric properties of which are consistent with the color observed. Films heated to 700 °C were orange in color, suggesting Ta_3N_5 , and also exhibited green opalescent regions when viewed from certain directions. The UV-vis transmission spectrum of one of these films (Figure 5) shows a dip in the transmission at 510–520

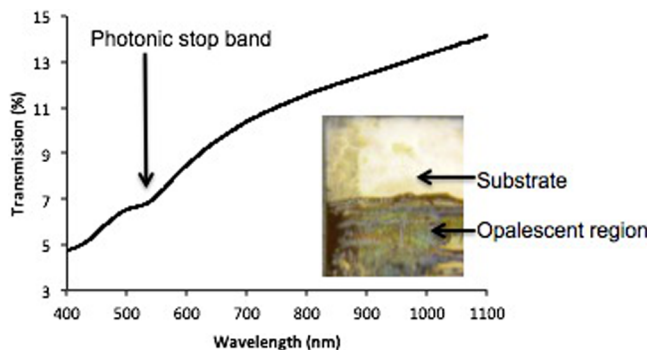


Figure 5. Transmission spectrum of an inverse opal film heated at 700 °C, and (inset) photograph showing one of the regions of the film displaying green opalescence due to the ordered porous structure.

nm that is consistent with the expected photonic stop band, superimposed on the general trend of steeply decreasing transmission below ~650 nm due to the band edge of the red Ta_3N_5 .³⁶ Films heated to 800 °C had a deep orange color but no opalescence due to disruption of the long-range ordering of the film shown in Figure 4. The film colors suggested that, similarly to the thin films, Ta_3N_5 was only crystallized at 700 and 800 °C, and the diffraction patterns (Figure 6) confirmed this to be the case. The observed peak widths are consistent with crystallite sizes of around 20 nm (Scherrer formula). Films heated to 600 °C contained broad peaks due to a nanocrystal-

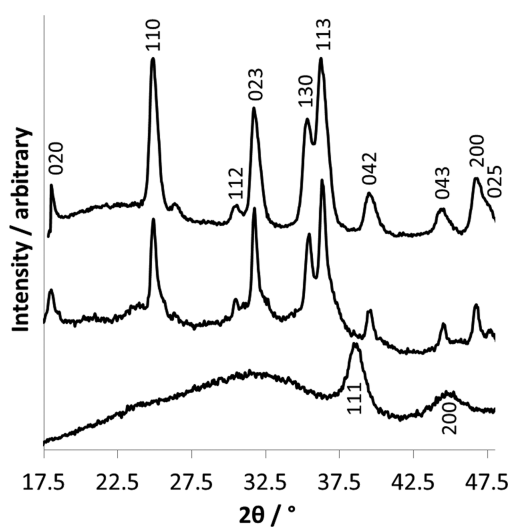


Figure 6. Patterns from inverse opal films heated to 600 (bottom), 700 (middle), and 800 °C (top) showing a broad amorphous background and broad peaks characteristic of nanocrystalline TaN at 600 °C and sharper Ta_3N_5 peaks at 700 and 800 °C. Major peaks are labeled with Miller indices.

line material with a rocksalt-type structure similar to cubic TaN (~7 nm crystallites) and a broad background suggesting some amorphous content.

EDX analysis of an inverse opal film heated to 700 °C confirmed tantalum, nitrogen and oxygen, and a strong silicon peak indicating that the beam was penetrating through to the substrate owing to the film thickness and the low volume fraction of solid in the porous films. Consequently, it is not possible to determine whether the detected oxygen originated entirely from the substrate or also from the film. The observed Ta:N ratio was ~1 in each analysis, which is significantly less than the 1.67 expected for Ta_3N_5 ; however due to the poor sensitivity to the probe to light elements the XRD characterization of Ta_3N_5 was considered more reliable. Film thicknesses were estimated by imaging a crack and measuring the close-packed pores (Figure 7); typical measured thicknesses were 5–10 μm, consistent with previous work.^{14,27}

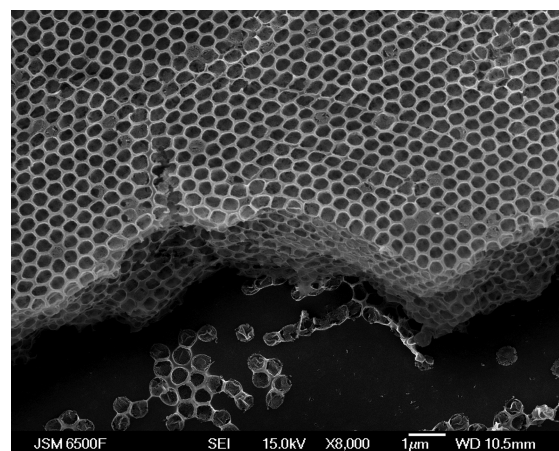


Figure 7. SEM image of a crack in a TaN inverse opal film heated at 600 °C, showing an approximate depth of 5 μm. Silica substrate is seen at the base of the edge, and note that the edge of the crack follows (110) planes of the hexagonal close-packed pores.

CONCLUSIONS

$Ta(NMe_2)_5$ undergoes rapid transamination reactions with *n*-propylamine, but self-condensation reactions occur less readily than shown in previous work using $Ti(NMe_2)_4$. Nonetheless, this is an effective system for the non-oxide sol-gel processing of Ta_3N_5 . Sols produced using 2 or more molar equivalents of *n*-propylamine were shown to condense irreversibly on solvent evaporation. Amidine-capped, divinylbenzene cross-linked polymer spheres that we previously demonstrated to be effective templates for such nonoxide sol-gel chemistry have now been assembled into close-packed templates with long-range order by temperature- and humidity-controlled evaporation of a suspension in water onto silica tiles. Infiltration of the nitride precursor sols was achieved by capillary action and evaporation, and the template was then cleanly removed by heating in ammonia. Ammonolysis at 600 °C removed the template but failed to crystallize Ta_3N_5 . At 700 °C well-ordered crystalline Ta_3N_5 inverse opal films were obtained, but at 800 °C ordering was lost as the samples started to anneal strongly.

ASSOCIATED CONTENT

Supporting Information

Thermogravimetric analysis of a tantalum nitride precursor xerogel and infrared spectra of a xerogel and a Ta₃N₅ inverse opal film. This material is available free of charge via the Internet at <http://pubs.acs.org>.

AUTHOR INFORMATION

Corresponding Author

*E-mail: A.L.Hector@soton.ac.uk.

Notes

The authors declare no competing financial interest.

ACKNOWLEDGMENTS

The authors thank EPSRC for support of B.M.G. via a doctoral training grant studentship and SAFC Hitech for a gift of Ta(NMe₂)₅.

REFERENCES

- (1) Norris, D. J.; Vlasov, Y. A. *Adv. Mater.* **2001**, *13*, 371.
- (2) Lee, K. T.; Lytle, J. C.; Ergang, N. S.; Oh, S. M.; Stein, A. *Adv. Funct. Mater.* **2005**, *15*, 547.
- (3) Scott, R. W. J.; Yang, S. M.; Chabanis, G.; Coombs, N.; Williams, D. E.; Ozin, G. A. *Adv. Mater.* **2001**, *13*, 1468.
- (4) Al-Daous, M. A.; Stein, A. *Chem. Mater.* **2003**, *15*, 2638.
- (5) Sung, I. K.; Mitchell, C. M.; Kim, D. P.; Kenis, P. J. A. *Adv. Funct. Mater.* **2005**, *15*, 1336.
- (6) (A) Tsang, M. Y. Macroporous semiconductors tantalum oxide, (oxy)nitride and nitride for photocatalytic hydrogen evolution. *M.Sc. thesis*; University of York, 2010. (B) Tsang, M. Y.; Pridmore, N. E.; Gillie, L. J.; Chou, Y. H.; Brydon, R.; Douthwaite, R. E. *Adv. Mater.* **2012**, *24*, 3406.
- (7) Gates, B.; Yin, Y.; Xia, Y. *Chem. Mater.* **1999**, *11*, 2827.
- (8) Yan, H.; Zhang, K.; Blanford, C. F.; Francis, L. F.; Stein, A. *Chem. Mater.* **2001**, *13*, 1374.
- (9) (A) Abdullah, M.; Iskandar, F.; Shibamoto, S.; Ogi, T.; Okuyama, K. *Acta Mater.* **2004**, *52*, 5151. (B) Carbajo, M. C.; Gomez, A.; Torralvo, M. J.; Enciso, E. J. *Mater. Chem.* **2002**, *12*, 2740.
- (10) (A) McLachlan, M. A.; Johnson, N. P.; de la Rue, R. M.; McComb, D. W. *J. Mater. Chem.* **2005**, *15*, 369. (B) McLachlan, M. A.; Barron, C. C. A.; Johnson, N. P.; de la Rue, R. M.; McComb, D. W. *J. Cryst. Growth* **2008**, *310*, 2644.
- (11) (A) Madhavi, S.; Ferraris, C.; White, T. *J. Solid State Chem.* **2006**, *179*, 866. (B) McLachlan, M. A.; McComb, D. W.; Ryan, M. P.; Morozovska, A. N.; Eliseev, E. A.; Payzant, E. A.; Jesse, S.; Seal, K.; Baddorf, A. P.; Kalinin, S. V. *Adv. Funct. Mater.* **2011**, *21*, 941.
- (12) Meseguer, F.; Blanco, A.; Míguez, H.; García-Santamaría, F.; Ibáñez, M.; López, C. *Colloids Surf. A: Physicochem. Eng. Aspects* **2002**, *202*, 281.
- (13) Rugge, A.; Becker, J. S.; Gordon, R. G.; Tolbert, S. H. *Nano Lett.* **2003**, *3*, 1293.
- (14) Rugge, A.; Park, J.; Gordon, R. G.; Tolbert, S. J. *Phys. Chem. B* **2005**, *109*, 3764.
- (15) Fischer, A.; Jun, Y.-S.; Thomas, A.; Antonietti, M. *Chem. Mater.* **2008**, *20*, 7383.
- (16) Subban, C. V.; Smith, I. C.; DiSalvo, F. J. *Small* **2012**, *8*, 2824.
- (17) Gray, B. M.; Hassan, S.; Hector, A. L.; Kalaji, A.; Mazumder, B. *Chem. Mater.* **2009**, *21*, 4210.
- (18) Jackson, A. W.; Hector, A. L. *J. Mater. Chem.* **2007**, *17*, 1016.
- (19) (A) Hector, A. L. *Chem. Soc. Rev.* **2007**, *36*, 1745. (B) Mazumder, B.; Hector, A. L. *J. Mater. Chem.* **2009**, *19*, 4673.
- (20) Hassan, S.; Hector, A. L.; Kalaji, A. *J. Mater. Chem.* **2011**, *21*, 6370.
- (21) Cheng, F.; Kelly, S. M.; Clark, S.; Bradley, J. S.; Baumbach, M.; Schütze, A. *J. Membr. Sci.* **2006**, *280*, 530.
- (22) Rocher, V.; Kelly, S. M.; Hector, A. L. *Microporous Mesoporous Mater.* **2012**, *156*, 196.
- (23) Hassan, S.; Hector, A. L.; Hyde, J. R.; Kalaji, A.; Smith, D. C. *Chem. Commun.* **2008**, 5304.
- (24) Farrusseng, D.; Schlichte, K.; Spliethoff, B.; Wingen, A.; Kaskel, S.; Bradley, J. S.; Schüth, F. *Angew. Chem., Int. Ed.* **2001**, *40*, 4204.
- (25) Moriya, Y.; Takata, T.; Domen, K. *Coord. Chem. Rev.* **2013**, *257*, 1957.
- (26) Fang, C. M.; Orhan, E.; de Wijs, G. A.; Hintzen, H. T.; de Groot, R. A.; Marchand, R.; Saillard, J. Y.; de With, G. J. *Mater. Chem.* **2001**, *11*, 1248.
- (27) Granqvist, C. G. *Adv. Mater.* **2003**, *15*, 1789.
- (28) Ishikawa, A.; Takata, T.; Kondo, J. N.; Hara, M.; Domen, K. J. *Phys. Chem. B* **2004**, *108*, 11049.
- (29) Tabata, M.; Maeda, K.; Higashi, M.; Lu, D.; Takata, T.; Abe, R.; Domen, K. *Langmuir* **2010**, *26*, 9161.
- (30) Zhang, Q.; Gao, L. *Langmuir* **2004**, *20*, 9821.
- (31) Feng, X.; LaTempa, T. J.; Basham, J. I.; Mor, G. K.; Varghese, O. K.; Grimes, C. A. *Nano Lett.* **2010**, *10*, 948.
- (32) Dang, H. X.; Hahn, N. T.; Park, H. S.; Bard, A. J.; Mullins, C. B. *J. Phys. Chem. C* **2012**, *116*, 19225.
- (33) Baxter, D. V.; Chisholm, M. H.; Gama, G. J.; DiStasi, V. F.; Hector, A. L.; Parkin, I. P. *Chem. Mater.* **1996**, *8*, 1222.
- (34) Shah, S. I. U.; Hector, A. L. *Top. Catal.* **2012**, *55*, 950.
- (35) (A) Brauer, G.; Weidlein, J. R. *Angew. Chem.* **1965**, *77*, 218. (B) Brese, N. E.; O'Keeffe, M.; Rauch, P.; DiSalvo, F. J. *Acta Crystallogr., Sect. C* **1991**, *47*, 2291.
- (36) Henderson, S. J.; Hector, A. L. *J. Solid State Chem.* **2006**, *179*, 3518.
- (37) Fix, R.; Gordon, R.; Hoffman, D. *Chem. Mater.* **1993**, *5*, 614.